Selective laser melting *In Situ* temperature monitoring using femtosecond point-by-point Fiber Bragg Gratings

Alexandre Lerner, Quentin Pouille, Ayoub Ladaci, Romain Cotillard, Fernando Lomello, Pascal Aubry, Hicham Maskrot, Géraud Bouwmans, Guillaume Laffont

Selective Laser Melting *In Situ* Temperature Monitoring Using Femtosecond Point-by-Point Fiber Bragg Gratings

Alexandre Lerner[1,2], Quentin Pouille[3], Ayoub Ladaci[3], Romain Cotillard[1], Fernando Lomello[3], Pascal Aubry[3], Hicham Maskrot[3], Géraud Bouwmans[2] and Guillaume Laffont[1]

[1]*Université Paris-Saclay, CEA, List, F-91120, Palaiseau, France*

[2]*Univ. Lille, CNRS, UMR 8523 – PhLAM – Physique des Lasers Atomes et Molécules, F-59000 Lille, France*

[3]*Université Paris-Saclay, CEA, Service d'Études Analytiques et de Réactivité des Surfaces, 91191, Gif-sur-Yvette, France*

alexandre.lerner@cea.fr

Abstract: Dynamic temperature monitoring along a stainless steel specimen additively manufactured by selective laser melting was performed using point-by-point written femtosecond Fiber Bragg Gratings packaged in a metallic capillary.

1. Introduction

The quality and materials properties of metallic parts produced by Additive Manufacturing (AM) depend on multiple process parameters specific to the selected technique. Selective Laser Melting (SLM) relies on the scanning of a powder bed by an intense laser beam and the subsequent melting and re-solidification of the metallic material to produce parts layer-by-layer.

Common *in situ* monitoring techniques of this process are optical-based methods (cameras, photodiodes, pyrometry) studying the metallic melt pool geometry, temperature or material discontinuities and defects [1,2]. X-rays based methods can be used to study in-depth material dynamics [3]. Acoustic methods allow *in situ* defect localization [4].

Thanks to their immunity to electromagnetic interferences, multiplexing capabilities and large temperature range of operation, Optical Fiber Sensors (OFSs) have been used to monitor AM processes. They can be used as direct (embedded in the manufactured part) or indirect (setup instrumentation) sensing probes.

Laser Engineering Net Shaping (LENS) distributed temperature monitoring was performed by Optical Frequency Domain Reflectometry (OFDR) using embedded nickel-coated optical fibers [5]. The embedding process of Ni-coated Fiber Bragg Gratings (FBGs) based OFSs on a custom-made SLM setup was performed by Havermann [6]. FBGs placed inside the SLM build chamber allow *in situ* porosity detection by acoustic emission [7]. Finally, Hehr *et al*. report optical fibers embedded in an additively manufactured build plate to perform distributed strain monitoring of the SLM process by OFDR [8].

FBGs consist of a periodic refractive index modulation inscribed in the core of an optical fiber. According to a phase matching condition, they reflect a resonance band centered on λ_B, as per Eq. 1.

$$m\,\lambda_B = 2\,n_{eff}\,\Lambda \tag{1}$$

Where m is the harmonic order, Λ is the grating pitch and n_{eff} is the effective refractive index of the core guided electromagnetic mode. High temperature resistant FBGs can be written using femtosecond lasers. Specifically, tightly focused pulses generate micro-explosions in the material, resulting in a spherical void structure surrounded by a densified silica shell. These gratings are known as point-by-point (PbP) written FBGs and can operate to temperature up to 1000°C [9]. This technique also allows FBG writing through-the-coating (WTC) of optical fibers [10]. Processes involving extreme temperatures can be monitored using fs-PbP FBGs by following the Bragg Wavelength Shift (BWS), as was realized on a TIG weld bead by Cotillard *et al.* [11].

In this work, we used in-capillary strain-insensitive fs-PbP FBG arrays to monitor an SLM process. The sensors were embedded during the fabrication process allowing a dynamic *in situ* temperature monitoring of the metallic part.

2. Experimental procedure

2.1. Optical fiber sensors manufacturing

The OFSs array consisted of three 3 mm-long second order FBGs equally distributed over 30 mm (referenced as E1, E2 and E3). They were written PbP through the coating of a polyimide-coated single mode optical fiber (coating diameter ~155 µm) using a frequency doubled Yb femtosecond laser at CEA List LCFO facilities.

The FBGs array was inserted and centered in a ~50 mm long 316L stainless steel (SS) capillary of 0.2 mm internal and 0.4 mm external diameter. The fiber was secured in position using a ceramic glue dot on one end of the capillary such as the OFSs array was insensitive to external strain.

2.2. *Embedding procedure by selective laser melting*

The SLM printer was a TRUMPF TruPrint Series 1000 operated at CEA DES LISL facilities. The specimen was printed from a 316L powder and was 50 mm in length, 5 mm in width and 5 mm in height. Layer height was 30 µm.

The embedding process is presented in Fig. 1. First, the lower part of the specimen comprising a Ø500 µm groove was printed, removed from the printer, and cleaned out of the remaining unmelted powder (Fig. 1a). Secondly, the packaged in-capillary FBGs array was positioned in the groove and micro-welded to the lower part (Fig. 1b). Finally, the latter was re-positioned in the 3D printer and the manufacturing process was resumed to print the upper part of the specimen (68 layers) and to embed the FBGs array (Figs. 1c and 1d).

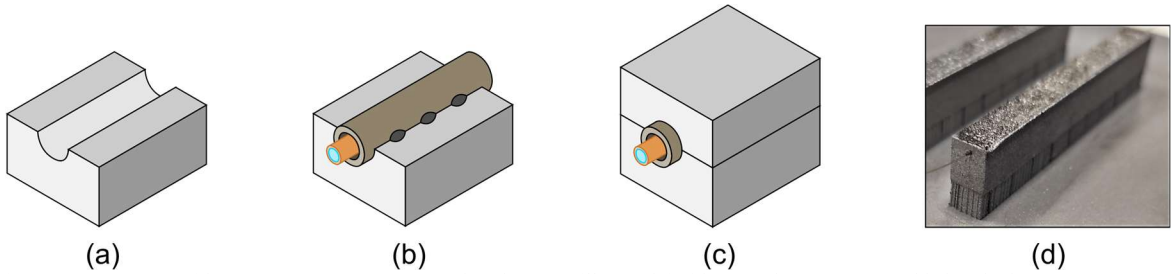

Fig 1. (a) Lower part with Ø500 µm groove (not to scale). (b) In-capillary polyimide-coated FBGs array welded to the lower part. (c) Upper part printing for sensor embedding. (d) Finished part after unmelted powder removal.

2.3. *Dynamic temperature monitoring*

BWS and spectral responses of the FBGs array were continuously monitored during the SLM process using a si255 optical sensing instrument (LUNA Innovations). Peaks position were recorded at 5 kHz (onboard peak detection algorithm) and spectral responses (1500–1580 nm, 20 pm resolution) were acquired in parallel at 10 Hz. Peaks position were also extracted from the spectral responses using a 3-dB bandwidth (BW) algorithm [12], as well as their Full Width at Half Maximum (FWHM) and amplitude.

Relative temperature shifts (ΔT) were calculated from BWS using a polynomial function determined from the calibration of an identical FBGs array in a vertical furnace. Note that the wavelength reference values for BWS calculation were acquired shortly before starting the laser scanning.

3. Results and Discussion

3.1. *Full process temperature monitoring*

The laser scan for each printed layer (68 in total) along the specimen lead to successive heating of the FBGs along the sensors array (Fig. 2). Peak temperature is reached when the laser beam is directly over the sensor. The maximum temperature elevation measured during the process was 459°C by FBG E3. It is much lower than the melt pool temperature above, which may exceed 1900°C [13], because of the thermal insulation induced by the 100 µm-thick capillary, ~15 µm polyimide coating and the air gap in-between. Nonetheless, each temperature peak is sufficiently time resolved to be considered as input data for an inverse heat transfer model in order to retrieve the thermal flux generated by the melt pool above [14]. The baseline level increase up to approximately 100°C is due to heat accumulation by conduction in the substrate plate throughout the process.

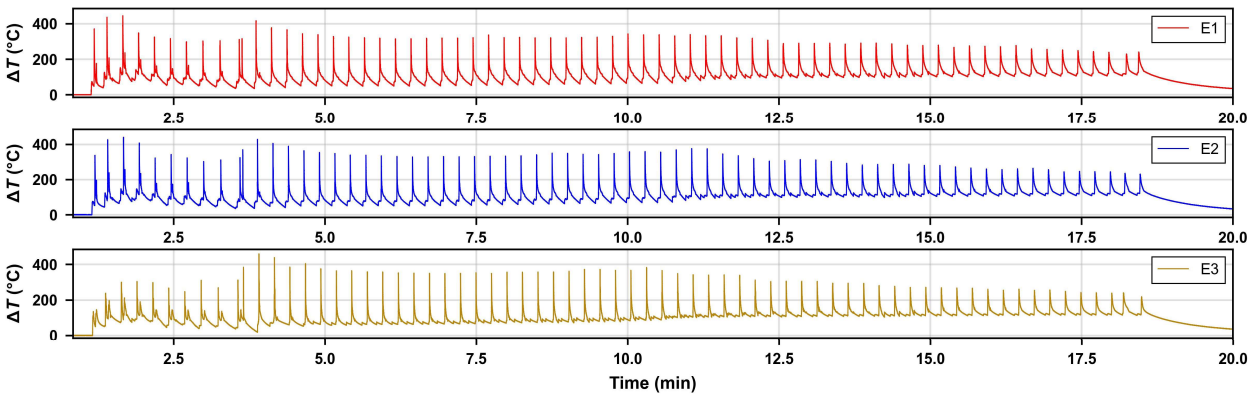

Fig. 2. Temperature *in situ* monitoring at 5 kHz throughout the upper part of the specimen manufacturing by SLM.

3.2. *Process dynamics*

One can observe that the temperature peaks corresponding to the first ten layers (t < 3.6 min in Fig. 2) present amplitude variations and doubling. The latter is attributed to the laser scan strategy, as these layers are printed in two times, *i.e.* one heat deposition on each side of the in-capillary sensors. The lower peak amplitude for FBG E3 during the printing of these layers may be caused by a misalignment of the capillary with regard to the Ø500 µm groove axis.

Temperature peaks induced by laser scanning are relatively consistent in shape from layer #11 until the end of the process. These layers are printed by a single laser scan along the surface of the specimen.

This scan along the longitudinal axis (duration ~5.5 s per 50×5 mm^2 layer) induces temperature gradients along the OFSs array. Reflected spectra for a single layer printing are presented in Fig. 3a, where strong peak chirping can be observed for each 3 mm-long FBG successively. Chirping magnitude may be reduced by writing shorter FBGs, and its profile may be further analyzed to determine the local temperature gradient. Peaks positions calculated by the 3-dB BW algorithm from three extracted spectra are also plotted in Figs. 3b–d.

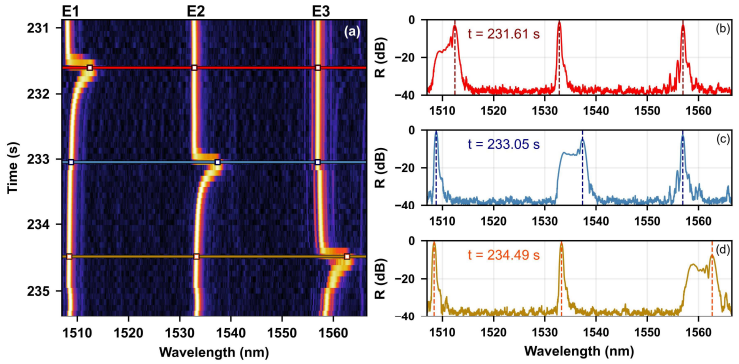

Fig. 3. (a) Reflected spectra amplitude as a function of time and wavelength for layer #11. (b)–(d) Spectra for maximum BWS of the different FBGs in the timespan. Vertical lines represent peaks position calculated with the 3-dB BW algorithm.

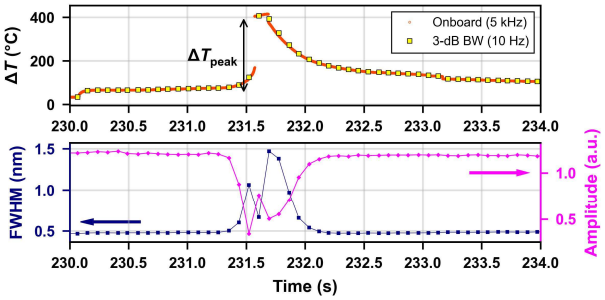

Fig. 4. Measured temperature and spectral characteristics of FBG E1 for a single laser scan (layer #11).

Peak detection accuracy under these severe thermal gradients must be addressed to further discuss the temperature measurements. Fig. 4 compares the on-board peak detection algorithm and the extracted peak positions from the spectral responses and presents the peak spectral characteristics (FWHM and amplitude) for one laser scan over FBG E1. Peak chirping is characterized by a FWHM increase from 0.5 to 1.5 nm. Even under severe spectral distortions, it can be noted that the two peak detection methods converge to close values. One can note that maximum peak temperature is acquired but the heating process is too fast compared to the peak acquisition frequency. In order to obtain a more complete description of the process's thermal dynamics, a higher sampling frequency of at least 10 kHz would be necessary.

Temperature dynamics measured by the buried sensors are driven by the heat input at the surface and the subsequent thermal transfers occurring inside the material. From layer #11, the deposited energy is identical at each laser scan.

Fig. 5a present baseline corrected temperature increases ΔT_{peak} induced by laser scanning above the sensors throughout the process from layer #11. Constant heating amplitude can be observed from layers #20 to #37, followed by a gradual decrease from layer #37 to #68 (last layer). A change in cooling dynamics can also be noted at this layer. Normalized temperature evolution ($\Delta T(t)/\Delta T_{peak}$) after maximum peak temperature was fitted by an exponential decay function ($e^{-\tau/t}$, where t is time). The corresponding time constant τ is presented in Fig. 5b. It globally increases with increasing number of layers, but a inflection can be observed at layer #37.

The increasing consolidated SS thickness above the buried sensor leads to lower peak temperature near the capillary (thermal insulation) and, consequently, an increase of the time constant τ. Nonetheless, the plateau observed in ΔT_{peak} for layers #20 to #37, as well as the inflection in τ near layer #37 shows that external factors affect the temperature measured in the capillary, which require further analysis of the process dynamics and heat transfer phenomena involved.

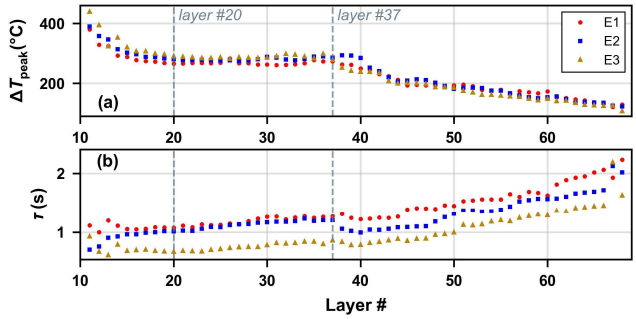

Fig. 5. (a) Baseline-corrected heat elevation induced by laser scanning over the FBGs for layers #11–68. (b) Time constant for exponential decay fit performed on normalized temperature evolution at cooling over 3.5 s.

4. Conclusion

Complete process monitoring of a few-millimeters thick 316L specimen manufactured by SLM additive manufacturing was performed using an in-capillary polyimide coated fs-PbP written FBGs array. The heating dynamics were shown to be too fast compared to the FBG sampling rate. Nonetheless, peak temperature and cooling dynamics could be reliably acquired. The latter were shown to be dependent on the material thickness above the buried sensor for a constant energy input, but complementary transient heat transfer and SLM specific thermal processes analysis shall be pursued to fully interpret the acquired data. Process thermal modeling is under investigation and the calculated results will be compared to the presented dataset. This work paves the way for *in situ* monitoring of the SLM process using high temperature resistant fs-PbP FBGs arrays directly embedded in the metallic material, as well as to perform Structural Health Monitoring on the instrumented parts designed to operate in harsh environments.

5. References

[1] S. Clijsters, T. Craeghs, S. Buls, K. Kempen, and J.-P. Kruth, "*In situ* quality control of the selective laser melting process using a high-speed, real-time melt pool monitoring system," Int J Adv Manuf Technol **75**, 1089–1101 (2014).

[2] S. K. Everton, M. Hirsch, P. Stravroulakis, R. K. Leach, and A. T. Clare, "Review of *in-situ* process monitoring and *in-situ* metrology for metal additive manufacturing," Materials & Design **95**, 431–445 (2016).

[3] C. L. A. Leung, S. Marussi, R. C. Atwood, M. Towrie, P. J. Withers, and P. D. Lee, "*In situ* X-ray imaging of defect and molten pool dynamics in laser additive manufacturing," Nature Communications **9**, 1355 (2018).

[4] N. Eschner, L. Weiser, B. Häfner, and G. Lanza, "Development of an Acoustic Process Monitoring System for Selective Laser Melting (SLM)," in *2018 International Solid Freeform Fabrication Symposium* (University of Texas at Austin, 2018).

[5] R. Zou, X. Liang, Q. Chen, M. Wang, M. A. S. Zaghloul, H. Lan, M. P. Buric, P. R. Ohodnicki, B. Chorpening, A. C. To, and K. P. Chen, "A Digital Twin Approach to Study Additive Manufacturing Processing Using Embedded Optical Fiber Sensors and Numerical Modeling," Journal of Lightwave Technology **38**, 6402–6411 (2020).

[6] D. Havermann, "Study on fibre optic sensors embedded into metallic structures by selective laser melting," Thesis, Heriot-Watt University (2015).

[7] S. A. Shevchik, G. Masinelli, C. Kenel, C. Leinenbach, and K. Wasmer, "Deep Learning for *In Situ* and Real-Time Quality Monitoring in Additive Manufacturing Using Acoustic Emission," IEEE Transactions on Industrial Informatics **15**, 5194–5203 (2019).

[8] A. Hehr, M. Norfolk, D. Kominsky, A. Boulanger, M. Davis, and P. Boulware, "Smart Build-Plate for Metal Additive Manufacturing Processes," Sensors **20**, 360 (2020).

[9] A. Martinez, I. Y. Khrushchev, and I. Bennion, "Thermal properties of fibre Bragg gratings inscribed point-by-point by infrared femtosecond laser," Electronics Letters **41**, 176–178 (2005).

[10] A. Martinez, I. Y. Khrushchev, and I. Bennion, "Direct inscription of Bragg gratings in coated fibers by an infrared femtosecond laser," Opt. Lett., OL **31**, 1603–1605 (2006).

[11] R. Cotillard, G. Laffont, S. Rougeault, D. Ayrault, O. Asserin, and R. Robidet, "Strain monitoring at high temperature by femtosecond point-by-point fiber Bragg Grating across a TIG weld bead," in *26th International Conference on Optical Fiber Sensors* (Optical Society of America, 2018), p. ThB3.

[12] D. Tosi, "Review and Analysis of Peak Tracking Techniques for Fiber Bragg Grating Sensors," Sensors **17**, 2368 (2017).

[13] Y. Li, K. Zhou, P. Tan, S. B. Tor, C. K. Chua, and K. F. Leong, "Modeling temperature and residual stress fields in selective laser melting," International Journal of Mechanical Sciences **136**, 24–35 (2018).

[14] J. Gaspar, Y. Corre, M. Firdaouss, J. L. Gardarein, J. Gerardin, J. P. Gunn, M. Houry, G. Laffont, T. Loarer, M. Missirlian, J. Morales, P. Moreau, C. Pocheau, and E. Tsitrone, "First heat flux estimation in the lower divertor of WEST with embedded thermal measurements," Fusion Engineering and Design **146**, 757–760 (2019).